Signatures of Bloch-Band Geometry on Excitons: Nonhydrogenic Spectra in Transition-Metal Dichalcogenides

Ajit Srivastava* and Ataç Imamoğlu
Institute of Quantum Electronics, ETH Zürich, CH-8093 Zürich, Switzerland
(Received 15 July 2015; published 16 October 2015)

The geometry of electronic bands in a solid can drastically alter single-particle charge and spin transport. We show here that collective optical excitations arising from Coulomb interactions also exhibit unique signatures of Berry curvature and quantum geometric tensor. A nonzero Berry curvature mixes and lifts the degeneracy of $l \neq 0$ states, leading to a time-reversal-symmetric analog of the orbital Zeeman effect. The quantum geometric tensor, on the other hand, leads to l-dependent shifts of exciton states that is analogous to the Lamb shift. Our results provide an explanation for the nonhydrogenic exciton spectrum recently calculated for transition-metal dichalcogenides. Numerically, we find a Berry curvature induced splitting of ~10 meV between the $2p_x \pm i2p_y$ states of WSe_2.

DOI: 10.1103/PhysRevLett.115.166802 PACS numbers: 73.21.-b, 03.65.Vf, 71.35.Cc, 78.67.-n

Introduction.—An exciton, comprised of a bound electron-hole pair, is an elementary optical excitation of a semiconductor. In most semiconductors, a large dielectric constant and small effective masses of charge carriers result in a weakly bound exciton with a Bohr radius much larger than the lattice constant. Such excitons are termed as Wannier-Mott excitons and play a central role in understanding the optical response of a number of condensed-matter systems [1,2]. Although the charge carriers in a semiconductor are described by Bloch waves, excitonic spectra of most semiconductors resemble that of a hydrogen atom consisting of a Rydberg series [3]. At a first glance, this is surprising since the wave functions of electrons and holes in a solid obey crystal symmetry. For example, discrete translational symmetry in a crystal implies that single-particle band dispersions of electrons and holes are periodic in crystal momentum $\mathbf{k}$, necessarily making their kinetic energy nonparabolic. Nevertheless, in a semiconductor with a direct band gap at the Γ point ($\mathbf{k} = 0$) and large Bohr radius such that exciton is made from $\mathbf{k}$ states close to band minima, full symmetry of vacuum is restored, and a hydrogenic spectrum for excitons is obtained.

It was recently reported that in monolayers of semiconducting transition-metal dichalcogenides (TMDs) such as MoS_2 and WS_2, excitonic spectra deviates strongly from the hydrogenic Rydberg series [4–7]. In particular, states with identical principal quantum numbers, such as $2s$ and $2p$, are not degenerate [8–10]. Moreover, the degeneracy of $2p$ states was also found to be lifted in tight-binding calculations [11]. These exciting predictions were attributed to nonlocal dielectric screening in TMDs where the exciton Bohr radius of the $1s$ exciton is comparable to the monolayer thickness [12]. In fact, as a consequence of the tightly bound nature of Wannier-Mott excitons in this material system, the exciton comprises electron-hole states which are spread over a large momentum range where a parabolic description of the dispersion is not valid. Since TMD excitons are composed of electron-hole states around $\pm K$ points where Berry curvature is finite, it is natural to ask if Bloch-band geometry can alter the excitonic spectrum. While the role of Berry curvature in determining transport properties of noninteracting Bloch electrons is well established [13,14], its role in modifying Coulomb attraction leading to bound-state formation has not been explicitly analyzed.

In this Letter, we analyze the excitonic signatures of the two geometric invariants of Bloch bands—Berry curvature and a quantum geometric tensor (QGT). We show that the Berry curvature, acting as a momentum-space magnetic field [15] is responsible for a finite splitting of the $2p_x \pm i2p_y$ states. Very simply, in two dimensions, an out-of-plane Berry curvature is associated with circulating single-particle electron and hole states. Thus, when $l \neq 0$ exciton states are formed, states with a sense of rotation consistent with the direction of Berry curvature will have lower energy as compared to counterrotating states, thereby causing a splitting between the two. The QGT, on the other hand, contributes to the $2s$-$2p$ splitting, which is similar to the Lamb shift. Our findings apply to Wannier-Mott excitons in general, and are particularly relevant for TMD excitons where optical spectroscopy can directly probe the above-mentioned signatures of the Bloch-band geometry.

Exciton problem in momentum space.—The exciton motion can be decomposed into the relative motion of electron and hole giving rise to hydrogenlike bound states, and the center-of-mass momentum ($K_{\mathrm{c.m.}}$) resulting in an excitonic dispersion periodic in a reciprocal lattice vector. As light emission and absorption takes places around $K_{\mathrm{c.m.}} = 0$ due to the negligible momentum of photons, in the following we will only consider excitons with zero center-of-mass momentum. Without loss of generality, we

restrict ourselves to two-dimensional excitons for the rest of the discussion. The exciton wave function can be expressed as $\sum_{\mathbf{k}} A_\nu(\mathbf{k}) c^\dagger_{c,\mathbf{k}} c_{v,\mathbf{k}}|0\rangle = \sum_{\mathbf{k}} A_\nu(\mathbf{k})|\mathbf{k}\rangle$, with c_c (c_v) being the annihilation operator for an electron in the conduction (valence) band, and $|0\rangle$ being the semiconductor vacuum with no excitations. The $A_\nu(\mathbf{k})$ amplitudes satisfy the eigenvalue equation $\sum_{\mathbf{k}'}\langle\mathbf{k}|\mathcal{H}+V|\mathbf{k}'\rangle A_\nu(\mathbf{k}') = EA_\nu(\mathbf{k})$, where $\mathcal{H} = \sum_{\mathbf{k}} \mathcal{E}^v_{\mathbf{k}} c^\dagger_{v,\mathbf{k}} c_{v,\mathbf{k}} + \sum_{\mathbf{k}} \mathcal{E}^c_{\mathbf{k}} c^\dagger_{c,\mathbf{k}} c_{c,\mathbf{k}}$ is the single-particle Hamiltonian of the two-band semiconductor, and $V = \int d^2r d^2r' \Psi^\dagger(\mathbf{r})\Psi^\dagger(\mathbf{r}')(e^2/\varepsilon|\mathbf{r}-\mathbf{r}'|)\Psi(\mathbf{r})\Psi(\mathbf{r}')$ is the Coulomb interaction. Field operators are defined as $\Psi(\mathbf{r}) = (1/\sqrt{S})\sum_{n=v,c}\sum_{\mathbf{k}} u_{n,\mathbf{k}}(\mathbf{r}) e^{i\mathbf{k}\cdot\mathbf{r}} c_{n,\mathbf{k}}$, where $u_{n,\mathbf{k}}(\mathbf{r})$ are the Bloch functions of the band with index $n = c, v$, and S is the quantization area.

The matrix elements are given by $\langle\mathbf{k}|\mathcal{H}|\mathbf{k}'\rangle = \delta_{\mathbf{k},\mathbf{k}'}(\mathcal{E}^c_{\mathbf{k}} - \mathcal{E}^v_{\mathbf{k}})$, and $\langle\mathbf{k}|V|\mathbf{k}'\rangle = -(e^2/S^2)\int d^2r d^2r' u^*_{c,\mathbf{k}}(\mathbf{r}) u_{c,\mathbf{k}'}(\mathbf{r})(e^{i(\mathbf{k}'-\mathbf{k})\cdot(\mathbf{r}-\mathbf{r}')}/\varepsilon|\mathbf{r}-\mathbf{r}'|) u^*_{v,\mathbf{k}'}(\mathbf{r}') u_{v,\mathbf{k}}(\mathbf{r}') = -(1/S)(2\pi e^2/\varepsilon)(1/|\mathbf{k}-\mathbf{k}'|)\langle u_{c,\mathbf{k}}|u_{c,\mathbf{k}'}\rangle\langle u_{v,\mathbf{k}'}|u_{v,\mathbf{k}}\rangle$, which is the direct part of the Coulomb interaction. The long-range part of the exchange interaction of V vanishes for excitons with $K_{\text{c.m.}} = 0$. We neglect the short-range part of the exchange interaction since its magnitude is much smaller than the direct terms that we analyze. The eigenvalue equation for the exciton then becomes

$$(\Delta_{\mathbf{k}} - E_\nu)A_\nu(\mathbf{k}) - \frac{1}{S}\sum_{\mathbf{k}'} \frac{2\pi e^2}{\varepsilon|\mathbf{k}-\mathbf{k}'|} s^c_{\mathbf{k},\mathbf{k}'} s^v_{\mathbf{k}',\mathbf{k}} A_\nu(\mathbf{k}') = 0, \tag{1}$$

where the index $\nu = 1s$, $2s$, $2p$, etc., in analogy to the hydrogenic orbitals, $\Delta_{\mathbf{k}} = \mathcal{E}^c_{\mathbf{k}} - \mathcal{E}^v_{\mathbf{k}}$, ε is the nonlocal (screened) dielectric constant, and Bloch overlaps $s^n_{\mathbf{k},\mathbf{k}'} = \langle u_{n,\mathbf{k}}|u_{n,\mathbf{k}'}\rangle$. When the Bloch overlaps are unity, the dispersion $\Delta_{\mathbf{k}}$ is parabolic, and the dielectric constant is local, we recover the two-dimensional (2D) hydrogen atom as the solution. It is then clear that the nonhydrogenic behavior of the exciton arises from the breakdown of the above-mentioned assumptions. As the role of nonparabolicity and the nonlocal dielectric constant is well understood, in the following we focus on the effect of Bloch overlaps leading to a nonhydrogenic exciton spectra.

Bloch part: General arguments.—Equation (1) shows that Bloch overlaps $s^n_{\mathbf{k},\mathbf{k}'}$ enforce the symmetry of the crystal on Coulomb attraction between the electron-hole pair. The radial symmetry of hydrogen atom is lowered when $s^n_{\mathbf{k},\mathbf{k}'}$ deviates significantly from unity, thereby necessarily making the excitonic spectrum nonhydrogenic. Note that Bloch overlaps as defined above are gauge dependent unlike the eigenenergies E_ν. They need not change with band dispersion but depend on how the Bloch functions are arranged in $\mathbf{k}$ space or the geometry of Bloch bands $u_{n,\mathbf{k}}$ over the Brillouin zone. Guided by this observation, below we express $s^n_{\mathbf{k},\mathbf{k}'}$ in terms of geometric invariants of Bloch bands such as Berry curvature. We first note that the Bloch overlap $s^n_{\mathbf{k},\mathbf{k}'}$ for $\mathbf{k}' \sim \mathbf{k} + d\mathbf{k}$ can be expressed as

$$s^n_{\mathbf{k},\mathbf{k}+d\mathbf{k}} = 1 + \langle u_n(\mathbf{k})|\partial_{k_i}|u_n(\mathbf{k})\rangle dk_i + \frac{1}{2}\langle u_n(\mathbf{k})|\partial_{k_i}\partial_{k_j}|u_n(\mathbf{k})\rangle dk_i dk_j + \cdots. \tag{2}$$

The first order term in $d\mathbf{k}$ is the Berry connection $i\mathcal{A}_i$, which is related to the Berry curvature as $\Omega(\mathbf{k}) = \nabla\times\mathcal{A}(\mathbf{k})$ [13]. Equation (2) is not gauge invariant in that it does not transform as a tensor under the transformation $\tilde{u}_n(\mathbf{k}) = u_n(\mathbf{k})e^{i\alpha(\mathbf{k})}$. However, if one chooses a closed path in $\mathbf{k}$ space, arbitrary phases which arise under the $U(1)$ gauge transformation mutually cancel each other to give gauge-invariant quantities. Indeed, only such closed-loop terms appear in the characteristic polynomial of the eigenvalue problem in Eq. (1). It can be shown that, up to second order in $d\mathbf{k}$ [16],

$$\langle u_{\mathbf{k}_1}|u_{\mathbf{k}_2}\rangle\ldots\langle u_{\mathbf{k}_{N-1}}|u_{\mathbf{k}_N}\rangle \sim e^{[i\oint\mathcal{A}\cdot d\mathbf{k} - (1/2)\int g_{ij}dk_i dk_j]} \tag{3}$$

for a closed path, such that $u_{\mathbf{k}_N} = u_{\mathbf{k}_1}$. The first exponential on the rhs is nothing but the Berry phase of the closed path, while the second term in the exponential is the squared "length" of the path defined in terms of the quantum geometric tensor $g_{ij} = \text{Re}[\langle\partial_{k_i}u(\mathbf{k})|\partial_{k_j}u(\mathbf{k})\rangle] - \mathcal{A}_i\mathcal{A}_j$. The QGT, also referred to as the Fubini-Study metric, is a gauge-invariant quantity corresponding to the second order derivative in Eq. (2) which measures the infinitesimal distance between the Bloch states parametrized by $\mathbf{k}$ [17]. Thus, the gauge-invariant Bloch overlaps over a closed loop can be expressed solely in terms of geometric quantities characterizing the Bloch bands. It is instructive to study the effect of Bloch overlaps perturbatively, for which we consider an infinitesimal loop, when all $\mathbf{k}$'s are close to each other. Equation (3) then becomes

$$1 + i\Omega\cdot d\mathbf{S}_k - \frac{1}{2}g_{ij}dk_i dk_j + \cdots, \tag{4}$$

where we have expressed $\oint\mathcal{A}\cdot d\mathbf{k}$ in terms of the Berry curvature as $\int\Omega\cdot d\mathbf{S}_k$ using Stokes's theorem. The imaginary part of the above expression is proportional to the Berry curvature, which is an antisymmetric quantity, whereas the real part is proportional to the QGT, a symmetric quantity. When calculating Bloch overlaps for conduction and valence bands, the difference (sum) of the Berry curvatures (QGTs) of the two bands appears.

Illustrative model: Gapped graphene.—Having established a connection between the Bloch overlaps and the geometry of Bloch bands, we now illustrate how the Berry curvature and the QGT affect the exciton spectrum using a toy model. Consider a two-band model of graphene with a band gap at $\pm K$ points for which Bloch overlaps $s^n_{\mathbf{k},\mathbf{k}'}$ can

be analytically obtained. The Hamiltonian can be written in a Pauli basis of the two bands as $H(\mathbf{k}) = (atk_x, at\tau_v k_y, \Delta_0)$, where a is the lattice constant, t denotes the hopping energy, and $\tau_v = \pm 1$ is the valley index. The presence of inversion symmetry breaking band gap Δ_0 results in an equal but opposite Berry curvature near the valleys at the $\pm K$ points [18,19]. We assume that Δ_0 is large enough that the magnitude of Berry curvature at the $\pm K$ points $|\Omega_0| = a^2t^2/\Delta_0^2$ is small and can be taken to be constant in the $\mathbf{k}$ region where the exciton wave function extends, i.e., $\Omega_0|\mathbf{k}|^2 \ll 1$ for $|\mathbf{k}| \in \delta k \sim 1/a_B$ around the $\pm K$ points.

Under these assumptions,

$$s^c_{\mathbf{k},\mathbf{k}'} s^v_{\mathbf{k}',\mathbf{k}} = 1 + \frac{|\Omega_0|}{2}\left(i\tau_v(\mathbf{k}' \times \mathbf{k}) - \frac{1}{2}|\mathbf{k} - \mathbf{k}'|^2\right) + \cdots, \tag{5}$$

up to first order in $|\Omega_0|$. Thus, $|\Omega_0|$ serves as a small parameter for perturbative treatment of the Bloch part. Note that Eq. (5) is analogous to Eq. (4) for the present model. In particular, the imaginary, antisymmetric part (opposite in the two valleys) corresponds to the Berry curvature, while the real symmetric part corresponds to the QGT. Under the assumptions of the toy model, both the Berry curvature and the QGT are proportional to $|\Omega_0| = a^2t^2/\Delta_0^2$. Plugging Eq. (5) into Eq. (1), one can write the exciton Hamiltonian of Eq. (1) perturbatively as $H_{\text{ex}} = H^H + V^I$, where H^H is the Hamiltonian without the Bloch part describing the 2D hydrogen atom, while V^I is the perturbative term due to Bloch overlaps, which reads as

$$V^I = \frac{|\Omega_0|}{2}\frac{2\pi e^2}{S\varepsilon}\left(\frac{1}{2}|\mathbf{k} - \mathbf{k}'| - i\tau_v\frac{(\mathbf{k}' \times \mathbf{k})}{|\mathbf{k} - \mathbf{k}'|}\right). \tag{6}$$

We ignore the $\mathbf{k}$ dependence of ε to identify the contribution of the Bloch overlaps. The Hermitian operator V^I can be decomposed into a real, symmetric part, V^I_S, and an imaginary, antisymmetric part, V^I_{AS}.

In order to determine the new eigenvalues and eigenstates of the perturbed Hamiltonian, one needs to calculate the matrix elements of V_I in the basis of 2D hydrogenic levels. We first consider the effect of V^I on $2p_x$ and $2p_y$ states which are degenerate in the 2D hydrogen atom. Because of the symmetry of V^I_{AS} under the exchange of $\mathbf{k}$ and $\mathbf{k}'$, its diagonal matrix elements vanish, while the off-diagonal matrix elements are finite. Likewise, V^I_S only has diagonal matrix elements which are nonzero.

The new eigenstates are obtained by diagonalizing the following matrix:

$$\begin{pmatrix} E^H_{2p} + \langle\psi_{2p_x}|V^I_S|\psi_{2p_x}\rangle & \langle\psi_{2p_x}|V^I_{AS}|\psi_{2p_y}\rangle \\ \langle\psi_{2p_y}|V^I_{AS}|\psi_{2p_x}\rangle & E^H_{2p} + \langle\psi_{2p_y}|V^I_S|\psi_{2p_y}\rangle \end{pmatrix}. \tag{7}$$

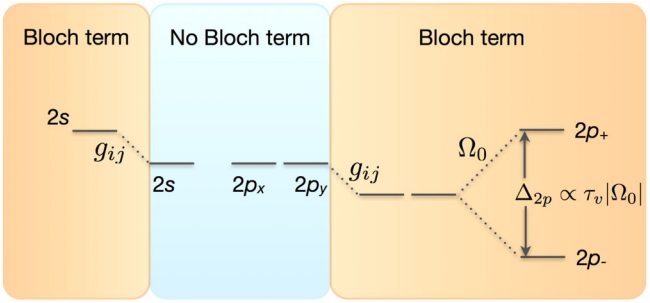

FIG. 1 (color online). A sketch of energy levels of the gapped-graphene model under assumptions of small, constant Berry curvature (Ω_0) and large exciton Bohr radius. In the absence of a Bloch term in the numerical calculations, $n = 2$ states remain degenerate, as with the hydrogen atom. Upon the inclusion of a Bloch term, the $2p$ states mix and split due to Ω_0, much like the orbital Zeeman effect. The shift in energy levels arises from the quantum geometric tensor (g_{ij}) and is analogous to Lamb shift in the hydrogen atom.

It is clear that the off-diagonal matrix elements arising from the antisymmetric part of the V^I will mix the $2p_x$ and $2p_y$ states into symmetric and antisymmetric combinations $|\psi_{2p_\pm}\rangle = (1/\sqrt{2})(|\psi_{2p_x}\rangle \pm i|\psi_{2p_y}\rangle)$, causing them to split. On the other hand, the diagonal matrix elements due to the symmetric part of V^I will cause a shift in energies of $|\psi_{2p_\pm}\rangle$ by the same amount.

Under the assumption of a small, constant Ω_0 and $\mathbf{k}$ close to the K point, we numerically evaluate the matrix elements in Eq. (7) to be $\langle\psi_{2p_x}|V^I_{AS}|\psi_{2p_y}\rangle = -i\tau_v|\Omega_0|c/2$ and $\langle\psi_{2p_x}|V^I_S|\psi_{2p_x}\rangle \sim -|\Omega_0|c/4$, where $c > 0$ is a constant. The energies of $2p_\pm$ states are obtained to be $E_{2p_\pm} = E_{2p} - |\Omega_0|c/4 \pm |\Omega_0|c/2$. The splitting between the $2p$ states is then $\Delta_{2p} \propto \tau_v|\Omega_0|$. For s states, only the symmetric part V^I_S survives, due to symmetry reasons, leading to a blueshift in energy. We find that the shift of $2s$ states is $\sim|\Omega_0|c/4$, making it almost degenerate with the $2p_+$ state, under our assumptions. Figure 1 shows a schematic energy-level diagram of the model with and without the Bloch perturbation. Upon setting the Bloch overlap to be unity, we find that the $2p$ states remain degenerate, resembling unmixed $2p_x$ and $2p_y$ orbitals, thereby confirming the role of Bloch overlaps in causing splitting.

Discussion.—The above scenario is an analog of the orbital Zeeman effect, where degeneracy of the $2p$ states of a hydrogen atom is lifted in the presence of a constant magnetic field due to a coupling to angular momentum l, an antisymmetric quantity. Berry curvature is the momentum-space analog of magnetic field, and the splitting here can be thought of as a "momentum-space orbital Zeeman effect." In general, the degeneracy of all $l \neq 0$ states of a 2D hydrogen atom will be lifted due to Berry curvature, as in the case of the orbital Zeeman effect. Because of the appearance of valley index τ_v in V^I_{AS}, the splitting is the opposite in the two valleys, as required by time-reversal symmetry. We emphasize that this splitting, which arises

from local (in reciprocal space) time-reversal symmetry breaking due to nonzero Berry curvature in the two valleys, *cannot* arise from nonlocal screening or nonparabolic dispersion which obeys time-reversal symmetry.

From Eq. (4), we can conclude that when Berry curvature is small but not constant, it is the Berry flux through the exciton wave function which determines the splitting. We note the similarity of our findings with that of Ref. [20], where excitons on the surface of topological insulators with explicitly broken time-reversal symmetry were considered.

One can also consider a two-band model with an identically zero Berry curvature to confirm that the mixing of $2p_x$ and $2p_y$ states stems from Berry curvature. If $(h_x(k_x,k_y), h_y(k_x,k_y), \Delta_0)$ is the Hamiltonian in a Pauli matrix basis, then choosing $h_x(k_x,k_y) \propto h_y(k_x,k_y)$ gives a vanishing Berry curvature, as it is proportional to $\partial h_x \times \partial h_y$. Indeed, in numerical calculations we find that the $2p$ wave functions for such a model remain unmixed.

Next, we comment on the role of the QGT in determining the exciton spectra. The QGT can be rewritten as

$$g_{ij} = \mathrm{Re}[\langle \partial_{k_i} u | \partial_{k_j u} \rangle] - \langle \partial_{k_i} u | u \rangle \langle u | \partial_{k_j} u \rangle = \langle X_i X_j \rangle - \langle X_i \rangle \langle X_j \rangle, \quad (8)$$

where the operator X is the generator of translation in the $\mathbf{k}$ space. The QGT then measures the quantum fluctuations of X [17]. In the present case, X corresponds to a spread in the relative position of the electron and the hole. This is not unlike the case of Lamb shift in a hydrogen atom where vacuum fluctuations of the electromagnetic field smear the electron's position, in turn changing its potential energy and resulting in a blueshift of its energy [21]. To make the analogy quantitative, we derive the dependence of the QGT related shift on the effective fine structure constant $\tilde{\alpha} = e^2/(\epsilon a t)$ and the mass gap Δ_0. As expected, we find a dependence which is similar to that for the hydrogenic Lamb shift, further confirming the analogy [16]. It is noteworthy that the magnitude of this Lamb-like shift can be relatively large compared to the hydrogenic Lamb shift; this observation can be thought of as a consequence of the fact that the effective fine structure constant of the gapped-graphene model, $\alpha = e^2/\hbar v$, is on the order of unity [22]. Even when Berry curvature vanishes identically, the effect of the QGT can still remain. Thus, we have identified another physically relevant consequence of the QGT, which has been previously shown to play a central role in such varied phenomena as electric polarization in insulators [23], current noise [14], superfluidity [24], fractional Chern insulators [25], and quantum phase transitions [26,27].

TMD excitons.—In the following, we investigate how the predictions of the preceding discussion apply to TMD excitons. We first note that the experimentally observed deviation from a hydrogenic series arises due to a combination of nonlocal dielectric screening, nonparabolic dispersion of bands, and the effect of the Bloch part. The assumption of constant and small Berry curvature no longer holds due to the large spread of exciton wave function in $\mathbf{k}$ space. In addition, unlike other material systems such as GaAs where the lowest energy exciton is made from electron-hole states near the Γ point ($\mathbf{k} = 0$), lowest energy excitons in TMDs are made from $\pm K$-point electron-hole pairs where there is nonzero Berry curvature. Thus, we expect a mixing and splitting of $2p$ states in addition to energy shifts due to the QGT.

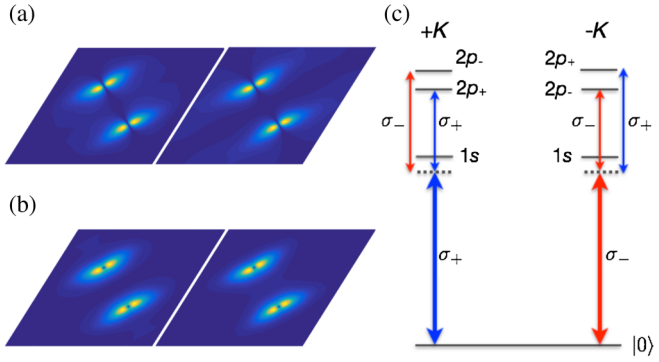

FIG. 2 (color online). Calculated squared amplitude of $2p$ wave functions in reciprocal space for MoS_2 in (a) the absence and (b) the presence of Bloch overlap. The Brillouin zone is chosen such that Γ points lie on the four vertices. The exciton wave function extends near the $\pm K$ points. Without the Bloch perturbation, the wave functions are degenerate and resemble $2p_x$ and $2p_y$ wave functions. Bloch perturbation mixes the states which resemble $2p_\pm$ states and have an energy splitting of about ~10 meV. (c) A sketch of energy levels with a scheme for optically determining the predicted splitting of $2p$ states using two-photon resonance spectroscopy.

We solve for the eigenvalue problem in Eq. (1) using a three-band, next-nearest neighbor model, for MoS_2 and WSe_2, which captures the band dispersion of conduction and the valence band throughout the Brillouin zone [28]. We discretize the Brillouin zone into a grid of 136×136 $\mathbf{k}$ points and assume an air-suspended sample with a nonlocal dielectric screening length $r^* \sim 15$ Å, corresponding to a binding energy of ~400 meV for the $1s$ state, which is estimated to be in the range of 300–700 meV [5,9,29]. The Coulomb part of the Hamiltonian is calculated such that $|\mathbf{k} - \mathbf{k}'|$ is always restricted to the first Brillouin zone.

Figures 2(a) and 2(b) show the $2p$ wave functions for a MoS_2 exciton with and without the Bloch part. As in the case of gapped graphene, $2p$ states remain unmixed without the inclusion of the Bloch part in the calculations. With the Bloch term included, we obtain a $2p$ splitting ~10 meV (~14 meV) for MoS_2 (WSe_2), which is consistent with the recently reported splitting of ~25 meV in MoS_2 [11]. Given the relatively large splitting, it should be possible to detect it experimentally using two-photon, polarization resolved optical spectroscopy involving a near-infrared laser slightly detuned from the $1s$ exciton and a midinfrared

laser, as shown in Fig. 2(c). When the two lasers are cocircularly (countercircularly) polarized, a lower (higher) energy $2p$ state will be excited in a two-photon resonance leading to an enhancement in photoluminescence from the $1s$ state. We note that even in the absence of a Bloch part, trigonal warping of the dispersion can lead to a degeneracy lifting between the $2p_x$ and $2p_y$ states; however, they remain unmixed and the magnitude of the splitting is much smaller than the Berry curvature induced splitting. We also note that the level diagram in Fig. 2(c) is strictly true for $K_{\mathrm{c.m.}} = 0$, as the long-range part of the exchange interaction will mix the states in opposite valleys for a finite $K_{\mathrm{c.m.}}$ [30].

Conclusions.—The central role played by the Berry curvature in determining the transport properties of noninteracting Bloch electrons, leading to anomalous valley and spin Hall effects, is well established. Our results, on the other hand, unequivocally demonstrate that the spectrum of Coulomb-correlated two-particle bound states exhibit observable signatures of Berry curvature and the QGT. This leads to the question of whether many-body optical excitations of semiconductors, such as trions in a 2D electron system, are also influenced by effective gauge fields in solids arising due to the nontrivial geometry of the Bloch bands.

We thank Charles Grenier for the fruitful discussions. This work is supported by NCCR Quantum Science and Technology (NCCR QSIT), a research instrument of the Swiss National Science Foundation (SNSF).

Note added.—Recently, a manuscript appeared reporting similar results using an effective Hamiltonian for excitons [31].

*Corresponding author.
asriv30@emory.edu

[1] T. Byrnes, N. Y. Kim, and Y. Yamamoto, Nat. Phys. **10**, 803 (2014).
[2] S. Smolka, W. Wuester, F. Haupt, S. Faelt, W. Wegscheider, and A. Imamoglu, Science **346**, 332 (2014).
[3] T. Kazimierczuk, D. Frohlich, S. Scheel, H. Stolz, and M. Bayer, Nature (London) **514**, 343 (2014).
[4] K. He, N. Kumar, L. Zhao, Z. Wang, K. F. Mak, H. Zhao, and J. Shan, Phys. Rev. Lett. **113**, 026803 (2014).
[5] A. Chernikov, T. C. Berkelbach, H. M. Hill, A. Rigosi, Y. Li, O. B. Aslan, D. R. Reichman, M. S. Hybertsen, and T. F. Heinz, Phys. Rev. Lett. **113**, 076802 (2014).
[6] M. M. Ugeda, A. J. Bradley, S.-F. Shi, F. H. da Jornada, Y. Zhang, D. Y. Qiu, W. Ruan, S.-K. Mo, Z. Hussain, Z.-X. Shen, F. Wang, S. G. Louie, and M. F. Crommie, Nat. Mater. **13**, 1091 (2014).
[7] B. Zhu, X. Chen, and X. Cui, Sci. Rep. **5**, 9218 (2015).
[8] Z. Ye, T. Cao, K. O'Brien, H. Zhu, X. Yin, Y. Wang, S. G. Louie, and X. Zhang, Nature (London) **513**, 214 (2014).
[9] G. Wang, X. Marie, I. Gerber, T. Amand, D. Lagarde, L. Bouet, M. Vidal, A. Balocchi, and B. Urbaszek, Phys. Rev. Lett. **114**, 097403 (2015).
[10] T. C. Berkelbach, M. S. Hybertsen, and D. R. Reichman, Phys. Rev. B **92**, 085413 (2015).
[11] F. Wu, F. Qu, and A. H. MacDonald, Phys. Rev. B **91**, 075310 (2015).
[12] T. C. Berkelbach, M. S. Hybertsen, and D. R. Reichman, Phys. Rev. B **88**, 045318 (2013).
[13] D. Xiao, M.-C. Chang, and Q. Niu, Rev. Mod. Phys. **82**, 1959 (2010).
[14] T. Neupert, C. Chamon, and C. Mudry, Phys. Rev. B **87**, 245103 (2013).
[15] H. M. Price, T. Ozawa, and I. Carusotto, Phys. Rev. Lett. **113**, 190403 (2014).
[16] See Supplemental Material at http://link.aps.org/supplemental/10.1103/PhysRevLett.115.166802 for the derivation of Eq. (3).
[17] J. P. Provost and G. Vallee, Commun. Math. Phys. **76**, 289 (1980).
[18] D. Xiao, W. Yao, and Q. Niu, Phys. Rev. Lett. **99**, 236809 (2007).
[19] W. Yao, D. Xiao, and Q. Niu, Phys. Rev. B **77**, 235406 (2008).
[20] I. Garate and M. Franz, Phys. Rev. B **84**, 045403 (2011).
[21] T. A. Welton, Phys. Rev. **74**, 1157 (1948).
[22] This shift arises due to the geometry of the Bloch bands in addition to the usual Lamb shift from the QED vacuum. The latter is expected to be orders of magnitude smaller due to the smallness of the fine structure constant.
[23] N. Marzari and D. Vanderbilt, Phys. Rev. B **56**, 12847 (1997).
[24] S. Peotta and P. Törmä, arXiv:1506.02815.
[25] M. Claassen, C. H. Lee, R. Thomale, X.-L. Qi, and T. P. Devereaux, Phys. Rev. Lett. **114**, 236802 (2015).
[26] Y.-Q. Ma, S. Chen, H. Fan, and W.-M. Liu, Phys. Rev. B **81**, 245129 (2010).
[27] P. Zanardi, P. Giorda, and M. Cozzini, Phys. Rev. Lett. **99**, 100603 (2007).
[28] G.-B. Liu, W.-Y. Shan, Y. Yao, W. Yao, and D. Xiao, Phys. Rev. B **88**, 085433 (2013).
[29] D. Y. Qiu, F. H. da Jornada, and S. G. Louie, Phys. Rev. Lett. **111**, 216805 (2013).
[30] H. Yu, G.-B. Liu, P. Gong, X. Xu and W. Yao, Nat. Commun. **5**, 3876 (2014).
[31] J. Zhou, W.-Y. Shan, W. Yao, and D. Xiao, following Letter, Phys. Rev. Lett. **115**, 166803 (2015).